DØ Note 6083-CONF

Search for Neutral Higgs Bosons at High $\tan\beta$ in the final state $\tau_\mu\tau_{\rm h}b$ with 4.3 fb^{-1} of Data

The DØ Collaboration
URL http://www-d0.fnal.gov
(Dated: July 19, 2010)

Data recorded by the DØ experiment at the Fermilab Tevatron Collider are analysed to search for neutral Higgs bosons produced in association with b quarks. This production mode can be enhanced in the minimal supersymmetric standard model (MSSM). The search is performed in the $\tau\tau b$ channel. The final state includes a muon, an hadronically decaying τ and a jet identified as coming from a b-quark. The analysed data set corresponds to an integrated luminosity of 4.3 fb^{-1} of Run2b data. The data are found to be consistent with background predictions and limits are set on the cross section times branching ratio and in the MSSM parameter space.

Preliminary Results for Summer 2010 Conferences

I. INTRODUCTION

Supersymmetry (SUSY) [1] is a popular extension of the standard model (SM) which overcomes the hierarchy problem of the SM. In contrast to the SM, where only one Higgs doublet is required to break the SU(2) symmetry, SUSY requires the presence of at least two Higgs doublets. In the MSSM five Higgs bosons remain after electroweak symmetry breaking; three neutral: h, H, and A - denoted as ϕ, and two charged: $H^{\pm}$. The Higgs sector can be parameterized by $\tan\beta$, the ratio of the two Higgs doublet vacuum expectation values, and m_A, the mass of the pseudo-scalar Higgs boson A.

The Higgs-quark couplings in the MSSM are proportional to their SM counterparts, with the exact factor depending on the type of quark (up- or down-type) and on the type of Higgs boson. For large values of $\tan\beta$ at least two Higgs bosons (either A and h, or A and H) have approximately the same mass and couplings to down-type quarks, which are enhanced by a factor $\tan\beta$ relative to the SM ones, while the couplings to up-type quarks are suppressed. In this large $\tan\beta$ region the three Higgs boson couplings follow the sum rule $g^2_{\mathrm{hbb}} + g^2_{\mathrm{Hbb}} + g^2_{\mathrm{Abb}} \approx 2 \times \tan^2\beta \times g^2_{\mathrm{hSM}}$. In $p\bar{p}$ collisions at $\sqrt{s} = 1.96$ TeV at the Fermilab Tevatron Collider, the production of Higgs bosons associated with bottom quarks (highest mass down-type quark) is therefore, enhanced by a factor $2 \times \tan^2\beta$ relative to the SM. Due to the $\tan\beta$ enhancement, the main decays for all these bosons are $\phi \to b\bar{b}$ and $\phi \to \tau^+\tau^-$ (the branching fractions are approximately $\mathcal{B}(\phi \to b\bar{b}) \approx 90$ % and $\mathcal{B}(\phi \to \tau^+\tau^-) \approx 10$ %). While the $b\bar{b}$ decay mode is strongly favoured, the subsequent final state suffers from a large multijet background making this channel challenging. The $b\tau\tau$ channel offers a cleaner final state. Compared to the inclusive Higgs production, that can be searched for in the $\tau\tau$ channel, the $b\tau\tau$ final state allows a strong suppression of the electroweak background due to the presence of the b-quark in the final state which makes this channel of particular interest for Higgs boson masses around the Z mass. We present a search for the final state with one muon originating from a tau decay, one calorimeter cluster originating from a tau decay and one b jet.

MSSM Higgs boson production has been studied at LEP which excluded $m_{h,A} < 93$ GeV/c^2 for all $\tan\beta$ values [2]. CDF [3, 4] and DØ [5–9] have extended the MSSM Higgs boson searches to higher masses for high $\tan\beta$ values. The result presented in this note extends an earlier DØ result [9]. In addition to including more data, this analysis benefits from improved techniques to discriminate signal from background.

The DØ detector is a general purpose detector described in Ref. [10]. We rely on all aspects of the detector: tracking, calorimetry, muon detection and secondary vertex identification.

II. DATA SET AND MONTE CARLO SAMPLES

Dedicated triggers designed to select events with at least one isolated muon with transverse momentum $p_T > 15$ GeV/c and pseudo-rapidity $|\eta| < 1.6$ are used in this analysis. The typical trigger efficiency for muons satisfying those kinematic conditions is about 60 %. The data used in this analysis were recorded between June 2006 and July 2009. After data quality requirements, the total data sample corresponds to an integrated luminosity 4.3 fb^{-1} [11].

Signal samples are generated for Higgs boson masses from 90-320 GeV/c^2. As the main difference between MSSM Higgs bosons and SM Higgs bosons is the MSSM enhancement, we use the leading order (LO) event generator PYTHIA [12] to generate SM associated production of ϕ and a b quark in the 5-flavor scheme, $gb \to \phi b$. Weights, calculated with MCFM [13], are applied to the signal samples as a function of p_T and η of the leading b jet which is not originating from the decay of the Higgs boson, to correct the LO cross section and kinematic distributions to next-to-leading order (NLO). When deriving the NLO kinematics and cross sections, we require $p_{Tb} > 12$ GeV/c and $|\eta_b| < 5$ on b quarks not originating from the Higgs boson.

The dominant sources of background are Z+jets, $t\bar{t}$ and multijet (MJ) production. In the MJ background the muon primarily comes from semileptonic b hadron decays, and not from τ decays. We also consider W+jets events and SM diboson production. Except for the MJ and W+jets contributions, all background yields are estimated using simulated events. The Z+jets, W+jets and $t\bar{t}$ samples are generated using ALPGEN [14]. The diboson samples are generated using PYTHIA.

The event generators are used conjointly with the CTEQ6L1 [15] parton distribution functions (PDF). ALPGEN samples are processed through PYTHIA for showering and hadronization. τ lepton decays are modelled via TAUOLA [16], and EVTGEN [17] is used to decay b hadrons. All samples are then passed through a GEANT-based [18] simulation of the DØ detector. Real data from a random beam crossing are added to `GEANT` events to model effects of detector noise, pileup, and additional $p\bar{p}$ interactions. The combined output is eventually processed through the same reconstruction algorithms as the data.

Corrections accounting for differences between data and the simulation are applied to the simulated events. The corrections are derived from control data samples and applied to object identification efficiencies, trigger efficiencies, primary $p\overline{p}$ interaction position (primary vertex), object energy scale, and the transverse momentum spectrum of Z bosons. After applying all corrections, the yields for signal and each background are calculated as the product of the acceptance (from the simulation) times the luminosity and predicted cross sections.

III. EVENT RECONSTRUCTION AND SELECTION

This analysis requires reconstruction of muons, hadronic decays of τ lepton ($\tau_{\rm h}$), b jets and missing transverse energy ($\not\!\!E_T$) arising from escaping neutrinos.

Muons are identified using track segments reconstructed in the muon system and are required to match a track reconstructed in the inner tracking system. Jets are reconstructed from energy deposits in calorimeter towers using the midpoint cone algorithm [19] with radius = 0.5. Jet reconstruction and energy scale determination are described in detail in Ref. [20]. All calorimeter jets are required to pass a set of quality criteria with about 98% efficiency and have at least two reconstructed tracks within $\Delta\mathcal{R}$(track, jet-axis) = $\sqrt{(\Delta\eta)^2 + (\Delta\varphi)^2} < 0.5$ (where η is the pseudorapidity and φ the azimuthal angle). Jets are also required to be consistent with originating from the primary vertex. A neural network (NN_b) based b-tagging algorithm [21], with lifetime based information involving the track impact parameters and secondary vertices as inputs, is used to identify b jets. Hadronic τ decays are identified [22] as energy deposits in the calorimeter, reconstructed with a jet cone algorithm $\mathcal{R} = 0.3$ [19], which have associated tracks. $\tau_{\rm h}$ candidates are then split in three different categories: one-prong τ decay with no π^0 s (called $\tau_{\rm h}$ type 1), one-prong decay with π^0 s ($\tau_{\rm h}$ type 2) and multiprong decay ($\tau_{\rm h}$ type 3). In addition, we use a neural network (NN_τ) based τ identification to separate quark or gluon jets from genuine $\tau_{\rm h}$ [22]. NN_τ is based on shower shape variables, isolation variables and correlation variables between the tracking and the calorimeter energy measurements. The $\not\!\!E_T$ is the negative of the vector sum of the transverse energy of calorimeter cells satisfying $|\eta| < 3.2$. We correct the $\not\!\!E_T$ for the energy scales of reconstructed final state objects, including muons.

A. Event preselection

In a first step we select a background-dominated sample by requiring:

- one primary vertex with at least three tracks
- exactly one isolated muon with $p_{T\mu} > 15$ GeV/c and $|\eta| < 1.6$;
- exactly one $\tau_{\rm h}$ with a transverse momentum, as measured in the calorimeter, $p_{T\tau_{\rm h}} > 10$ GeV/c, and $|\eta_{\tau_{\rm h}}| < 2.0$. Additionally, the tracks attached to the $\tau_{\rm h}$ candidate must satisfy: $\sum_{trk} p_{Ttrk} > 7/5/10$ GeV/c, where p_{Ttrk} is the track transverse momentum as measured in the tracker, for $\tau_{\rm h}$ type 1/2/3 respectively. For type 3, the leading track must have $p_T > 7$ GeV/c. $\tau_{\rm h}$ candidates matching any reconstructed muon within $\Delta\mathcal{R} < 0.5$ are discarded. $\tau_{\rm h}$ type 3 candidates, which can be associated with two or more tracks, must have an electric charge $q_{\tau_{\rm h}} \neq 0$. NN_τ >0.9/0.9/0.95 is required for $\tau_{\rm h}$ type 1/2/3 respectively; this tight identification criterion has an overall efficiency of ≈ 55 % in signal events for a fake rate of ≈ 2 % in multijet events;
- the electric charge of the selected $\tau_{\rm h}$, $q_{\tau_{\rm h}}$ must be opposite to the one of the selected muon, q_μ, *i.e.* $q_{\tau_{\rm h}} \times q_\mu < 0$
- at least one jet with $p_T > 15$ GeV/c, $|\eta| < 2.5$, $\Delta\mathcal{R}$(jet,$\tau_{\rm h}$) > 0.5 and $\Delta\mathcal{R}$(jet,μ) > 0.5;
- $m_T\,[W] < 100$ GeV/c^2, where $m_T\,[W] = \sqrt{2\,p_{T\mu}\,\not\!\!E_T\,(1 - \Delta\varphi[\mu;\not\!\!E_T])}$ with $\Delta\varphi[\mu;\not\!\!E_T]$ the azimuthal angle between the muon candidate and the $\not\!\!E_T$;
- $M_{vis} > 40$ GeV/c^2 (see Eq. 1).

The preselection sample is dominated by Z+jets, W+jets and MJ backgrounds. The MJ contribution is evaluated from data using different methods presented in the next section III B. The method used for determining the final result predicts W+jets and MJ backgrounds together. Tab. I gives the data and predicted background yields. Fig. 1 shows the invariant mass M_{vis} defined by:

$$M_{vis} = \sqrt{\left(|\vec{p}_\mu| + |\vec{p}_{\tau_{\rm h}}| + \not\!\!E_T\right)^2 - \left(\vec{p}_\mu + \vec{p}_{\tau_{\rm h}} + \vec{\not\!\!E}_T\right)^2}, \quad (1)$$

as well as the leading jet p_T.

	τ_h type 1	τ_h type 2	τ_h type 3	all types
$Z(\rightarrow \tau\tau)$	96.3 ± 5.3	676.1 ± 14.2	141.9 ± 6.0	914.2 ± 16.4
$Z(\rightarrow \tau\tau) + 2c$	4.3 ± 0.4	33.3 ± 1.2	5.2 ± 0.4	42.8 ± 1.3
$Z(\rightarrow \tau\tau) + 2b$	2.0 ± 0.2	15.6 ± 0.5	2.8 ± 0.2	20.4 ± 0.6
$Z(\rightarrow \mu\mu)$	11.6 ± 2.0	51.2 ± 3.6	11.7 ± 1.5	74.5 ± 4.4
$Z(\rightarrow \mu\mu) + 2c$	0.7 ± 0.2	4.1 ± 0.5	0.8 ± 0.2	5.6 ± 0.5
$Z(\rightarrow \mu\mu) + 2b$	0.3 ± 0.1	1.6 ± 0.2	0.4 ± 0.1	2.2 ± 0.2
$W(\rightarrow \mu\nu)$	16.8 ± 1.1	92.5 ± 3.1	54.0 ± 1.9	163.2 ± 3.8
$W(\rightarrow \mu\nu) + 2c$	0.6 ± 0.2	5.2 ± 0.6	3.5 ± 0.5	9.4 ± 0.8
$W(\rightarrow \mu\nu) + 2b$	0.3 ± 0.1	2.0 ± 0.2	1.1 ± 0.1	3.4 ± 0.3
$t\bar{t}$	5.1 ± 0.1	78.8 ± 0.4	5.6 ± 0.1	89.5 ± 0.5
diboson	2.7 ± 0.4	28.5 ± 1.2	3.5 ± 0.4	34.6 ± 1.4
MJ	42.1 ± 2.8	99.2 ± 5.6	110.2 ± 6.3	251.5 ± 8.9
Exp. Bkg	182.8 ± 6.5	1087.9 ± 16.2	340.6 ± 9.0	1611.3 ± 19.6
$DATA$	181	1065	346	1592
$HIGGS : m_\phi = 120GeV$	3.6 ± 0.3	25.2 ± 0.7	5.1 ± 0.3	33.9 ± 0.8

TABLE I: Expected background and observed yields at the preselection level. All errors are statistical only. The expected number of Higgs bosons corresponds to $\tan\beta = 40$ assuming MSSM tree-level enhancement and $\mathcal{B}(\phi \rightarrow \tau\tau) = 10$ %.

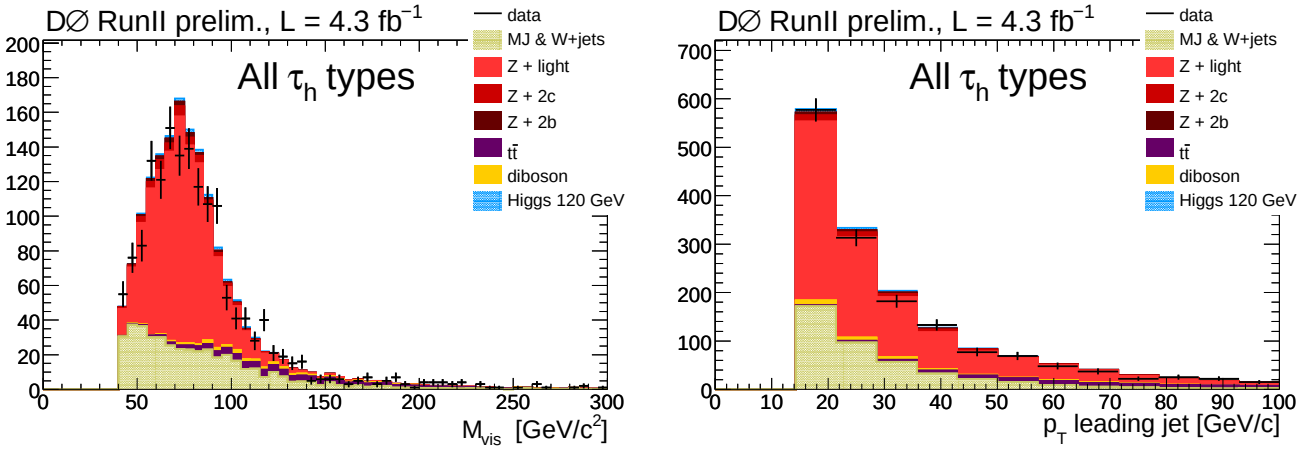

FIG. 1: Preselection: M_{vis} (left) and leading jet p_T distributions (all τ_h types).

B. Multijet (and W+jets) estimation

In the MJ and W+jets backgrounds, the muon candidate primarily comes from semileptonic decays of b hadrons and the τ_h candidate is faked by a jet.

We use three different methods to estimate MJ, W+jets or the sum of those two backgrounds:

- *the $f_{OS/SS}$ method.* The charge correlation between the muon and the τ_h candidates is expected to be small in the MJ background. Hence, we should have an equal amount of events with $q_{\tau_h} \times q_\mu < 0$ (OS for Opposite Sign) and $q_{\tau_h} \times q_\mu > 0$ (SS for Same Sign). The MJ background is determined from a data sample satisfying the preselection requirements except the charge correlation which is reversed. The other expected SM backgrounds are subtracted from the SS, and the number of MJ events in the OS (signal) sample is obtained by multiplying the SS sample by the OS:SS ratio, $f_{OS/SS}$, computed in a control sample selected by requiring a non-isolated muon. $f_{OS/SS}$ is found to be 1.06 ± 0.02. The W+jets background yield is determined from the simulation. Due to statistical limitations, this method can only be used at the preselection level.

- *the f_μ method.* The MJ background is expected to dominate non isolated muon samples. Therefore, we first determine the muon isolation fake rate, f_μ in a control sample selected by requiring $q_{\tau_\mathrm{h}} \times q_\mu > 0$ and $m_T\,[W] < 35$ GeV/c^2. The f_μ dependence on $E_\tau / \sum_{trk} p_{trk}$ and $p_{T\tau_\mathrm{h}}$ is measured and corrected for. The MJ background is then determined by applying f_μ to a non-isolated muon data sample selected with similar criteria as the preselection or the final selection except that the muon isolation is reversed. W+jets background has to be estimated from the simulation.

- *the f_τ method.* In this last method, we used data selected with similar cuts as the preselection or final selection except for NN_τ. Instead τ_h candidates must satisfy $NN_\tau < 0.2$. This sample is dominated by MJ and W+jets backgrounds. We subtract all the other SM backgrounds but W+jets using the simulation and apply τ_h fake rate, f_τ, to jets. f_τ has been measured in a data control sample satisfying similar criteria as the preselection level except that we drop the jet requirement and reverse the charge correlation. Therefore, both W+jets and MJ backgrounds are estimated jointly.

The three methods gives similar results on the background predictions. Since the f_τ method relies least on the simulation, it is eventually choosen as the nominal method.

C. Final selection

As a final step of the selection, at least one jet must satisfy a loose b-tag requirement $NN_b > 0.2$ with an identification efficiency of 71 % and a mistag rate of 16 % in Z+jets events. The data and expected backgrounds yields are given in Tab. II. This final selection is dominated by Z+jets, $t\bar{t}$ and MJ backgrounds.

Fig. 2 shows the invariant mass M_{vis} and the transverse momentum of the leading b-tag jet.

	τ_h type 1	τ_h type 2	τ_h type 3	all types
$Z(\rightarrow \tau\tau)$	15.8 ± 2.1	110.9 ± 6.5	26.0 ± 2.8	152.8 ± 7.4
$Z(\rightarrow \tau\tau) + 2c$	1.3 ± 0.2	10.7 ± 0.7	1.7 ± 0.3	13.7 ± 0.8
$Z(\rightarrow \tau\tau) + 2b$	1.2 ± 0.2	10.2 ± 0.4	1.7 ± 0.2	13.1 ± 0.5
$Z(\rightarrow \mu\mu)$	2.7 ± 1.1	8.1 ± 1.9	2.0 ± 0.9	12.7 ± 2.3
$Z(\rightarrow \mu\mu) + 2c$	0.2 ± 0.1	1.0 ± 0.2	0.2 ± 0.1	1.4 ± 0.3
$Z(\rightarrow \mu\mu) + 2b$	0.2 ± 0.1	1.0 ± 0.1	0.2 ± 0.0	1.3 ± 0.2
$W(\rightarrow \mu\nu)$	2.4 ± 0.4	14.1 ± 1.2	9.4 ± 0.9	25.9 ± 1.6
$W(\rightarrow \mu\nu) + 2c$	0.2 ± 0.2	1.6 ± 0.3	0.9 ± 0.3	2.7 ± 0.5
$W(\rightarrow \mu\nu) + 2b$	0.2 ± 0.0	1.2 ± 0.2	0.6 ± 0.1	1.9 ± 0.2
$t\bar{t}$	4.5 ± 0.1	68.6 ± 0.4	4.7 ± 0.1	77.8 ± 0.4
diboson	0.5 ± 0.2	5.0 ± 0.6	0.9 ± 0.2	6.4 ± 0.7
MJ	8.3 ± 1.2	25.7 ± 2.5	26.8 ± 3.0	60.8 ± 4.1
Exp. Bkg	37.4 ± 2.7	258.0 ± 7.4	75.1 ± 4.3	370.5 ± 9.0
$DATA$	37	259	76	372
$HIGGS : m_\phi = 120 GeV$	2.6 ± 0.2	17.8 ± 0.5	3.5 ± 0.2	23.9 ± 0.6

TABLE II: Expected background and observed yields in the final selection. All errors are statistical only. The expected number of Higgs bosons corresponds to $\tan\beta = 40$ assuming MSSM tree-level enhancement and $\mathcal{B}(\phi \rightarrow \tau\tau) = 10$ %.

IV. RESULTS

Since the final sample still suffers from a large background, we further improve the signal to background ratio by using neural network based discriminants against Z+jets, $t\bar{t}$ and MJ backgrounds. They are eventually combined into a final output from which limits are derived.

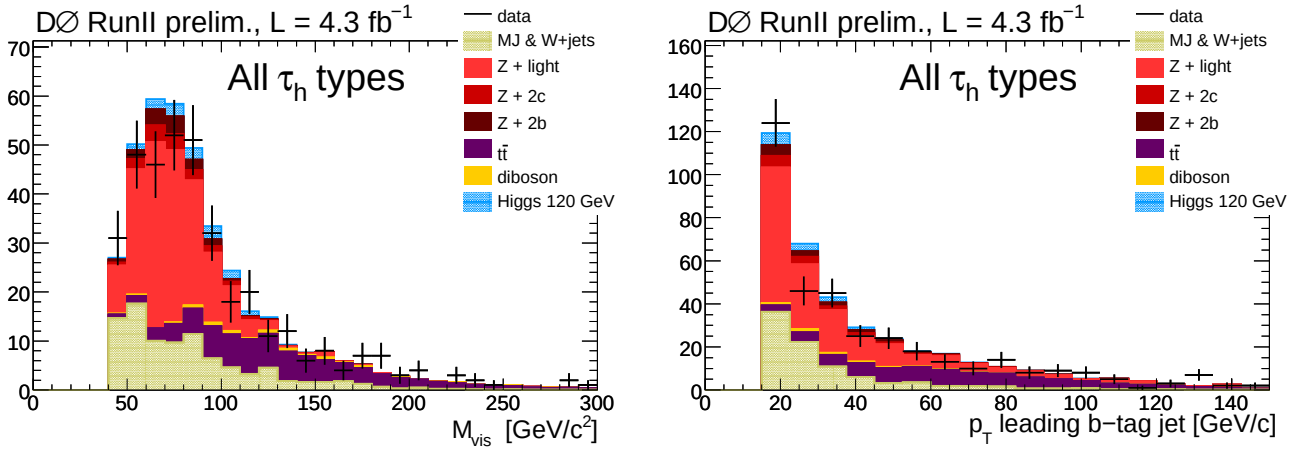

FIG. 2: Final selection: M_{vis} (left) and leading jet p_T distributions (all $\tau_{\rm h}$ types).

A. Multivariate methods

We define the transverse mass of a collection of N physical objects $m_T[O_1,...,O_k,...,O_N]$:

$$m_T[O_1,...,O_k,...,O_N] = \sqrt{\sum_{i=1}^{i\leq N}\sum_{j=1}^{j\leq N} p_T[O_i]\times p_T[O_j]\times(1-\cos\Delta\varphi[O_i;O_k])} \quad (2)$$

where $p_T[O_k]$ is the transverse momentum of the object O_k and $\Delta\varphi[O_i;O_j]$ is the azimuthal angle difference between the object O_i and O_j.

To separate the signal from the $t\bar{t}$ background we construct a discriminant,$\mathcal{D}_{t\bar{t}}$, for eight Higgs boson masses using the following variables: $|\Delta\varphi[\mu;\tau_{\rm h}]|$, $|\Delta\varphi[\mu;\not\!\!E_T]|$, $H_T \equiv \sum_{jets} p_T[jets]$, $E_T \equiv H_T + p_{T\tau_{\rm h}} + p_{T\mu}$, $\not\!\!E_T$, $m_T[\mu,\tau_{\rm h},\not\!\!E_T]$, $m_T[\mu,\tau_{\rm h},\not\!\!E_T,jets]$, $m_T[\mu,\not\!\!E_T]\mathcal{A}_T \equiv \frac{p_{T\mu}-p_{T\tau_{\rm h}}}{p_{T\tau_{\rm h}}}$ and the number of jets N_{jets}.

To separate the signal from the MJ background we construct a discriminant,$\mathcal{D}_{\rm MJ}$, for eight Higgs boson masses using the following variables: $p_{T\tau_{\rm h}}$, $p_{T\mu}$, $\not\!\!E_T$, $|\Delta\varphi[\mu;\tau_{\rm h}]|$, $|\Delta\varphi[\mu;\not\!\!E_T]|$, H_T, $m_T[\mu,\tau_{\rm h},\not\!\!E_T]$ and $m_T[\mu,\tau_{\rm h},\not\!\!E_T,jets]$.

To separate the signal from Z+light partons background, we use as discriminant $\mathcal{D}_{\rm lead-b}$, the NN_b output of the b-tagged jet with the highest transverse momentum.

Finally, we combine $\mathcal{D}_{t\bar{t}}$, $\mathcal{D}_{\rm MJ}$ and $\mathcal{D}_{\rm lead-b}$ into a final discriminant $\mathcal{D}_f$ obtained for eight different signal mass ranges and for each $\tau_{\rm h}$ type with the formula:

$$\mathcal{D}_f = (\mathcal{D}_{t\bar{t}}\times\mathcal{D}_{\rm MJ}\times\mathcal{D}_{\rm lead-b})^{\frac{1}{3}} \quad (3)$$

The lowest Higgs boson-mass discriminant $\mathcal{D}_f$ distributions are presented for all $\tau_{\rm h}$ types on Fig. 3.

B. Systematic uncertainties

Systematic uncertainties arise from a number of sources. Experimental uncertainties are evaluated by comparing data control samples to predictions from the simulation. We split the different sources into two categories: (1) those affecting only the normalisation, and (2) those which affect also the shape of the distributions. We include in the first category the uncertainty on the integrated luminosity (6.1 %), on the muon identification efficiency (2.9 %), on the trigger efficiency (5 %), on the $\tau_{\rm h}$ identification efficiency (12/4.3/7.7 % for $\tau_{\rm h}$ type 1/2/3 respectively), on the theoretical Z production cross section (4 %) on the Z+b and Z+c production cross sections (20 %), on the $t\bar{t}$ production cross section (11 %), on the $\tau_{\rm h}$ energy scale (0.1 %), on the jet energy scale ($3-7$ %), on the jet energy resolution (≈ 5 %), on the jet identification efficiency ($1-3$ %). The systematics affecting the shape of the output $\mathcal{D}_f$ are the uncertainty on the Z boson transverse momentum (≈ 6 %), and on the NN_b output of jets arising from b quarks ($2-4$ %), on the NN_b output of jets coming from light partons (up to 6 %), on the MJ $+Wjets$ evaluation ($20-50$ %).

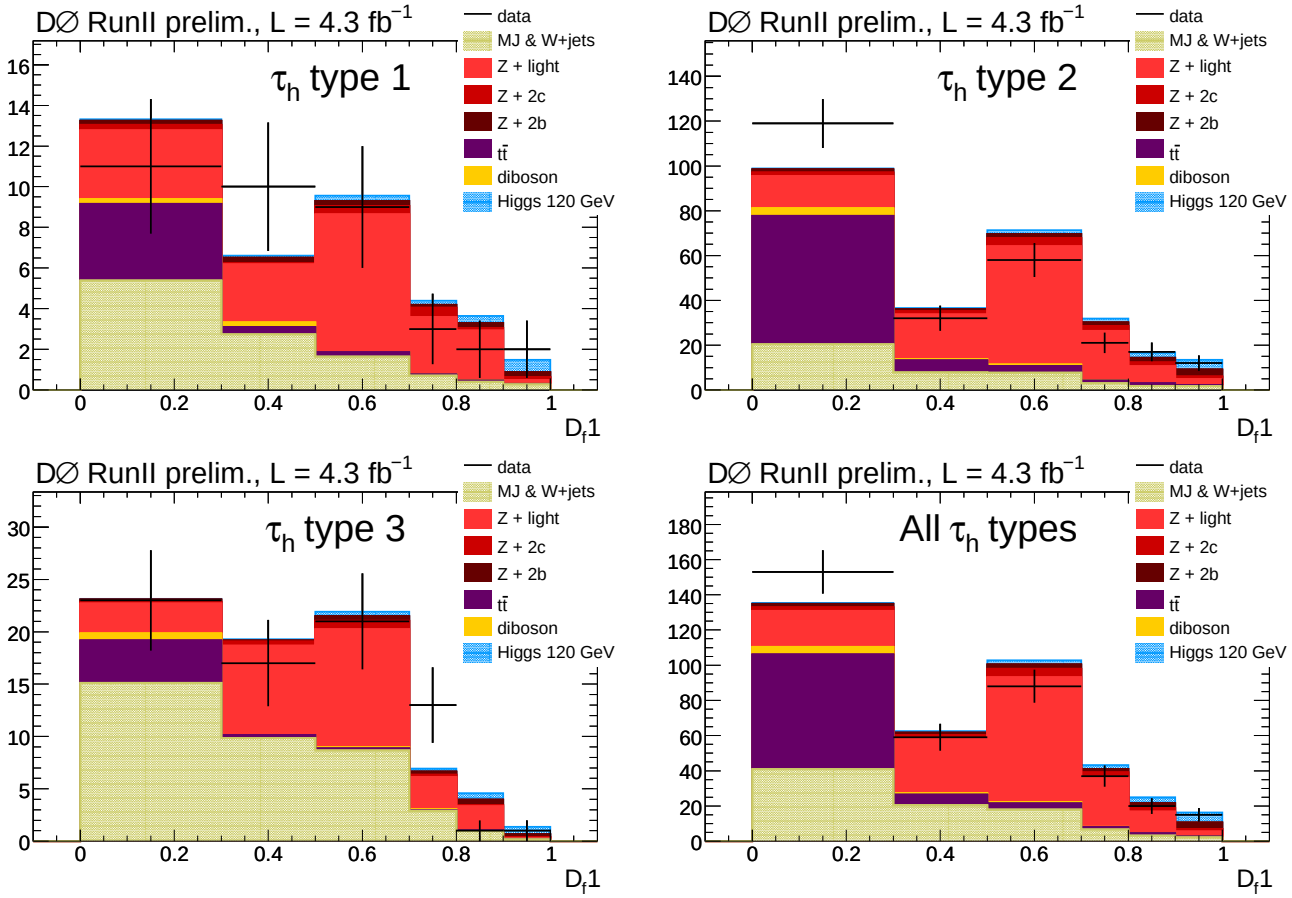

FIG. 3: $\mathcal{D}_f$ distributions for events containing a $\tau_{\rm h}$ type 1 (top left), $\tau_{\rm h}$ type 2 (top right), $\tau_{\rm h}$ type 3 (bottom left), all types together (bottom right) in the final selection. A MSSM Higgs signal with $m_\phi = 120$ GeV/c^2 and $\tan\beta = 40$ as been added to the total expected background (assuming tree-level enhancement).

C. Limits

$\mathcal{D}_f$ discriminants, as for example shown in Fig. 3, are used as input to a significance calculation using a modified frequentist approach with a Poisson log-likelihood ratio test statistic [23]. In the absence of a significant signal, we derive limits at the 95% confidence level on the cross section times branching ratio as a function m_A as shown in Fig. 4.

The cross section limits can be used to constrain the MSSM parameter space. As a consequence of the enhanced couplings to b quarks at large $\tan\beta$, the total width of the neutral Higgs boson also increases. We restrained our search to a MSSM parameters region where this effect can be neglected compared to the experimental resolution. An approximation of the MSSM cross section times branching ratio is given by [24]:

$$\sigma_{MSSM}(gb \to Ab) \times \mathcal{B}(A \to \tau^+\tau^-) \approx \sigma_{SM}(gb \to Ab) \times \frac{\tan^2\beta}{(1+\Delta_b)^2+9} \quad (4)$$

where the parameter Δ_b is due to radiative corrections, hence at tree-level $\Delta_b = 0$. This formula implies that the $\phi \to \tau^+\tau^-$ production is only moderately dependent on higher order calculation and we translate the cross section limits into $\tan\beta$ limits assuming $\Delta_b = 0$. The result is shown on Fig. 5.

In summary, we have reported a search for production of Higgs bosons decaying to tau pair in association with b quarks. The data are consistent with predictions from SM and we set limits on the neutral Higgs bosons production cross section times branching ratio. They are translated into limits on the MSSM parameter space using the tree-level approximation aforementioned. The constraints placed on $\tan\beta$ at low m_A are the most stringent to date obtained in a direct MSSM Higgs search.

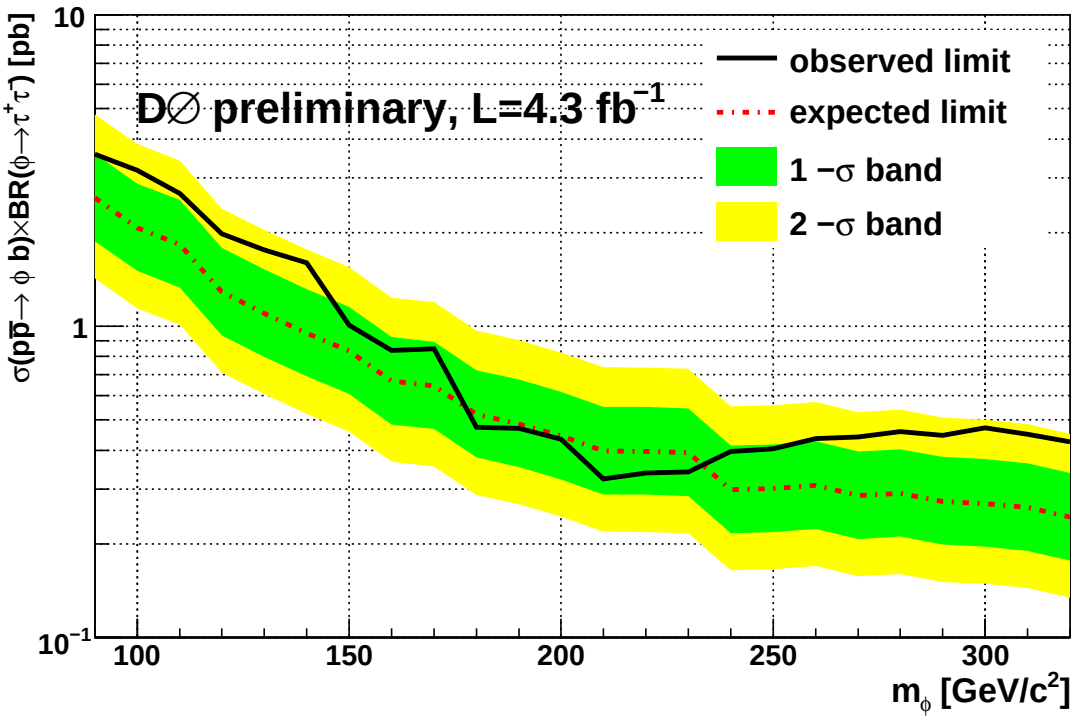

FIG. 4: Upper 95 % CL limits on the cross section times branching ratio as a function of m_ϕ. These model independent limits are derived assuming the width of the ϕ Higgs boson to be negligible relative to the experimental resolution.

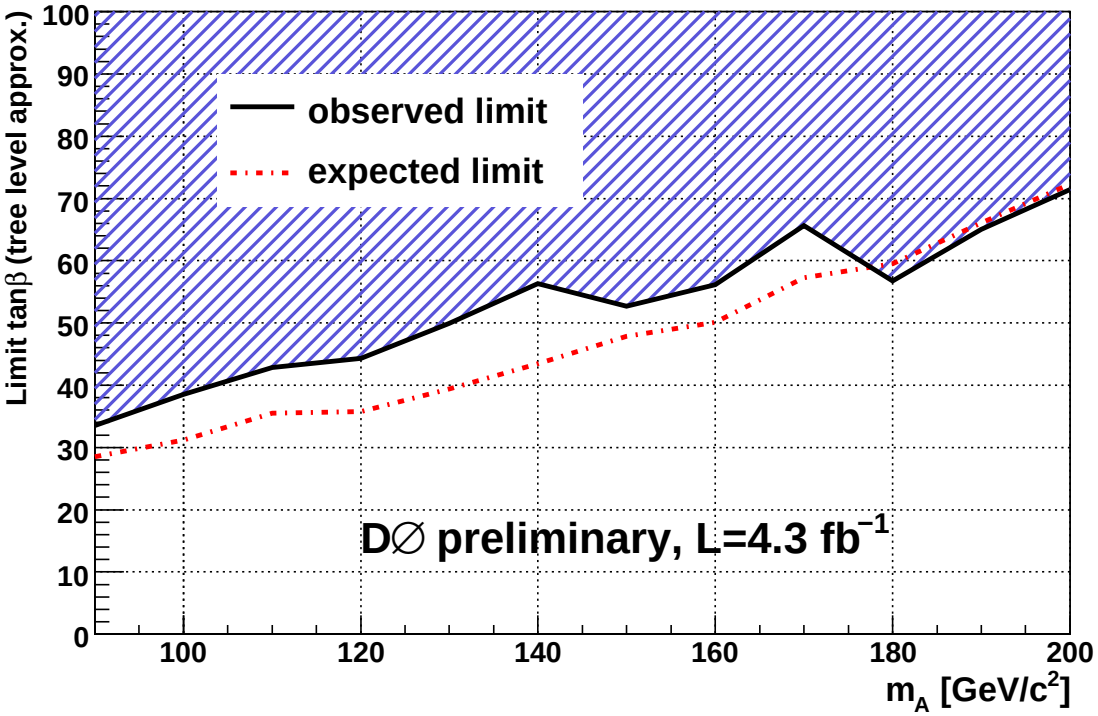

FIG. 5: Upper 95 % CL limits on $\tan\beta$ a function of the $\mathcal{CP}$-odd Higgs boson mass m_A. We assume a MSSM tree-level enhancement with respect to the SM cross section (see text) and we neglect the Higgs bosons width.

Acknowledgments

We thank the staffs at Fermilab and collaborating institutions, and acknowledge support from the DOE and NSF (USA); CEA and CNRS/IN2P3 (France); FASI, Rosatom and RFBR (Russia); CNPq, FAPERJ, FAPESP and FUNDUNESP (Brazil); DAE and DST (India); Colciencias (Colombia); CONACyT (Mexico); KRF and KOSEF (Korea); CONICET and UBACyT (Argentina); FOM (The Netherlands); STFC and the Royal Society (United Kingdom); MSMT and GACR (Czech Republic); CRC Program and NSERC (Canada); BMBF and DFG (Germany); SFI (Ireland); The Swedish Research Council (Sweden); and CAS and CNSF (China).

[1] H.P. Nilles, Phys. Rep. **110**, 1 (1984); H.E. Haber and G.L. Kane, Phys. Rep. **117**, 75 (1985).
[2] S. Schael *et al.* (The ALEPH, DELPHI, L3, and OPAL Collaborations), Eur. Phys. J. C **47**, 547 (2006).
[3] T. Affolder *et al.* (CDF collaboration), Phys. Rev. Lett. **86**, 4472 (2001).
[4] A. Abulencia *et al.* (CDF Collaboration), Phys. Rev. Lett. **96**, 011802 (2006).
[5] V.M. Abazov *et al.* (D0 Collaboration), Phys. Rev. Lett. **95**, 151801 (2005).
[6] V.M. Abazov *et al.* (D0 Collaboration), Phys. Rev. Lett. **101**, 071804 (2008).
[7] V.M. Abazov *et al.* (D0 Collaboration), Phys. Rev. Lett. **101**, 221802 (2008).
[8] V.M. Abazov *et al.* (D0 Collaboration), Phys. Rev. Lett. **102**, 051804 (2009).
[9] V.M. Abazov *et al.* (D0 Collaboration), Phys. Rev. Lett. **104**, 151801 (2010).
[10] V.M. Abazov *et al.* (D0 Collaboration), Nucl. Instrum. Methods Phys. Res. A **565**, 463 (2006).
[11] T. Andeen *et al.*, FERMILAB-TM-2365 (2007).
[12] T. Sjöstrand *et al.*, J. High Energy Phys. **05**, 026 (2006).
[13] J. Campbell, R.K. Ellis, F. Maltoni, and S. Willenbrock, Phys. Rev. D **67**, 095002 (2003).
[14] M.L. Mangano *et al.*, J. High Energy Phys. **307**, 001 (2003).
[15] CTEQ6 reference:
J. Pumplin *et al.*, JHEP **0207** 012 (2002) and D. Stump *et al.*, JHEP **0310** 046 (2003).
[16] Z. Was, Nucl. Phys. B - Proc. Suppl. **98**, 96 (2001). Version 2.5.04.
[17] D.J. Lange, Nucl. Instrum. Methods in Phys. Res. A **462**, 152 (2001). Version 9.39.
[18] R. Brun and F. Carminati, CERN program library long writeup W5013 1993 (unpublished). We use GEANT 3.
[19] G. Blazey *et al.*, arXiv:hep-ex/0005012 (2000).
[20] V.M. Abazov *et al.* (D0 Collaboration), Fermilab-Pub-08/034-E (2008).
[21] V.M. Abazov *et al.* (D0 Collaboration), Nucl. Instrum. Methods Phys. Res. A **620**, 400 (2010).
[22] V. M. Abazov *et al.* (D0 Collaboration), Phys. Lett. B **670**, 292 (2009).
[23] W. Fisher, FERMILAB report No. FERMILAB-TM-2386-E, 2007.
[24] M. Carena *et al.* arXiv:hep-ph/0511023v1